Transverse Single Spin Asymmetry via Charged Pion Production in Polarized p + p 200 GeV collisions at Midrapidity

by

Jae Hee Yoo

August 19, 2020

Abstract

Contents

Abstract **i**

Contents **iii**

List of Figures **vii**

List of Tables **ix**

1 Introduction **1**

1.1 Motivation 1

2 Data Selection **3**

2.1 Run Selection 3

2.1.1 RunQA by DAQ 3

2.1.2 RunQA by Spin Data Quality 3

2.2 Integrated Luminosity 4

2.3 $\pi^{\pm}$ Identification Cuts 4

3 QA and Calibration **7**

3.1 Warn Map in the EMCal 7

3.2 Dead Maps for DC, PC and RICH 7

3.3 Fiducial Cuts in the Central Arm 7

3.4 Matching Calibration in the EMCal and PC3 11

3.5 Polarization 11
3.6 Relative Luminosity 12
3.7 Azimuthal Correction 12

4 Cross Section Analysis **17**
4.1 $\pi^{\pm}$ Yields Extraction 17
4.2 Acceptance X Reconstruction Efficiency 17
4.3 Trigger Efficiency 17
4.4 Results 20

5 $\mathbf{A}_N$ Analysis **23**
5.1 A_N Calculation 23
5.1.1 Mean p_T 23
5.1.2 Square Root Formula 24
5.1.3 Relative Luminosity Formula 24
5.1.4 $sin\phi$ Modulation Cross Check 24
5.2 Background Subtraction 29
5.2.1 Background Fraction 29
5.2.2 Background Asymmetry 29
5.2.3 Results After Background Correction 29

6 Systematic Studies **31**
6.1 Uncertainty of Relative Luminosity 31
6.2 Global Scaling Uncertainty from Polarization 31
6.3 Bunch Shuffling 31
6.4 False Asymmetry from Ghost Cluster in the EMCal 31
6.5 Uncertainty from Background 31
6.6 Final Result 31

7 Conclusion **33**
7.1 The Section 33

Bibliography **35**

List of Figures

2.1 Run15 PP runs. Left plot represent DQA runtime and Right plot represent DQA livetime Red dotted lines mean DAQ cut. 4

3.1 EMCal 8 sectors warnmap. 8
3.2 Drift Chamber Deadmap. 8
3.3 Pad Chamber Deadmap. 9
3.4 RICH Deadmap. 10
3.5 ROC curve of failure detection 11
3.6 ROC curve of failure detection 11
3.7 Run 15 pp collision Polarization by fill. 12
3.8 Run 15 pp collision Relative Luminosity fill by fill and run by run. 12
3.9 Approximate appearance of Raw A_N and Azimuthal Acceptance Correction Formula. 13
3.10 phi distribution in 5 $\sim$ 6 GeV pT range 13
3.11 phi distribution in 6 $\sim$ 7 GeV pT range 14
3.12 phi distribution in 7 $\sim$ 8 GeV pT range 14
3.13 phi distribution in 8 $\sim$ 11 GeV pT range 15
3.14 phi distribution in 11 $\sim$ 15 GeV pT range 15
3.15 Azimutal Acceptance Correction Factor for Both Arms used for the square root formula and Relative Luminosity Formula in East and west arm, respectively. 16

4.1 $\pi^{\pm}$ Yields Extraction for run15 pp collision in central arm. 18
4.2 Generated $\pi^{\pm}$ distribution by using single particle generator. 18
4.3 Rec. X Acc. efficiency for $\pi^{\pm}$ by simulation. 19
4.4 Generated $\pi^{\pm}$ distribution by using single particle generator. 19
4.5 trigger efficiency for $\pi^{\pm}$ compared each dataset 20
4.6 trigger efficiency for $\pi^{\pm}$ with all dataset. 20
4.7 Cross Section for $\pi^{\pm}$ with Yuehang's 200GeV configuration file by using Pythia simulation. 21

5.1 Square Root Formula. 24
5.2 Relative Luminosity Formula. 25
5.3 A_N from different formula. 25
5.4 A_N compare with different charge. 25
5.5 Asymmetry as a function of ϕ for $5 < pT < 6$ GeV. 26
5.6 Asymmetry as a function of ϕ for $6 < pT < 7$ GeV. 26
5.7 Asymmetry as a function of ϕ for $7 < pT < 8$ GeV. 27
5.8 Asymmetry as a function of ϕ for $8 < pT < 11$ GeV. 27
5.9 Asymmetry as a function of ϕ for $11 < pT < 15$ GeV. 28
5.10 A_N Cross Check. 28

List of Tables

5.1 Finalized cut values, FoM 23

Chapter 1

Introduction

The single transverse-spin asymmetry (A_N) gives a clue to the transverse-spin structure of the proton, which can in turn provide some insight into the angular-momentum component of partons. Therefore, analysis of A_N of charged pions using central arm detectors in mid-rapidity region to study the transverse-spin structure functions of the proton by using pp collision.

1.1 Motivation

A proton is basically composed of many sea quarks and gluons in addition to the three valence quarks. According to the early EMC (European Muon Collaboration) data in 80's, the contribution of the three valence quarks to the whole proton's spin value (1/2) is less than 30%. As a result, the rest should come from gluons, sea quarks, and their orbital motions. The detailed spin structure of the proton can be revealed by investigating the longitudinal as well as the transversal components. In particular, the transverse-spin structure of the proton can provide some insight into the angular-momentum component of partons in the proton. QCD models predict that the transversal spin structure is originated from the transverse-momentum dependent Parton Distribution Functions (PDFs). About the origin of the transverse-spin asymmetry there are three possible explanations at the moment: the ‘Sivers’, ‘Collins’ and ‘higher twist’ effects. The Sivers effect is originated from an intrinsic kT imbalance in the initial parton distribution. On the other hand, the Collins effect generates the azimuthal single-spin asymmetry due to the modulation in the Collins fragmentation function at the hadronization stage. Finally, the higher-twist effect (twist-3) implies interference among gluon fields in the initial or final states within the collinear factorization limit.

TSSA measurements in p + p collisions are best described with twist-3 collinear correlation functions which can describe spin-momentum correlations both in the proton and in the process of hadronization. $\pi^+ = u\bar{d}$, $\pi^- = d\bar{u}$) the $\pi^{\pm}$. Because they are hadrons, they are sensitive to both initial- and final-state effects. Unlike at forward rapidity, midrapidity $\pi\,0$s are sensitive at leading order to gluon spin-momentum correlations both in the proton and in the process of hadronization.

Chapter 2

Data Selection

- Run15pp200CAERTP108
- Run15pp200CAMBP108
- Run15pp200CAFVTXP108
- Run15pp200CAMPCP108
- Run15pp200CAMUP108
- Run15pp200CAOTP108

2.1 Run Selection

2.1.1 RunQA by DAQ

RunQA by using runtime cut (>10 min) and livetime cut(> 0.5).

- ERT_4x4c&BBCLL1(noVtx)

2.1.2 RunQA by Spin Data Quality

In spin DB, there are strange fills or runs.

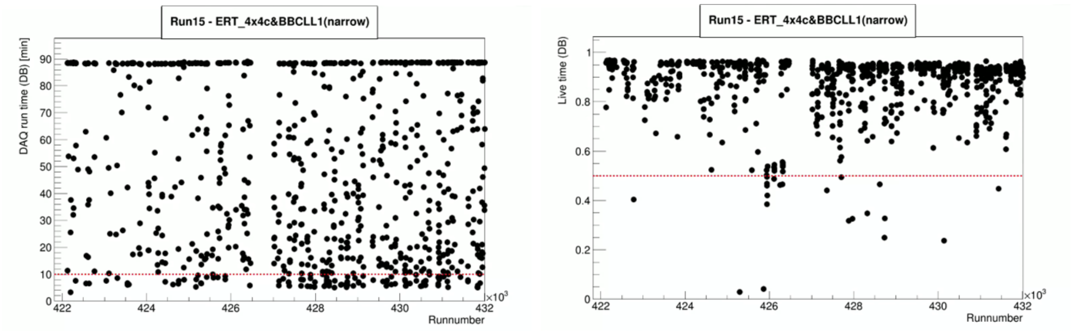

Figure 2.1: Run15 PP runs. Left plot represent DQA runtime and Right plot represent DQA livetime Red dotted lines mean DAQ cut.

2.2 Integrated Luminosity

For calculate Crosssection analysis.

$$\int Ldt = \frac{N^i_{ERTC\_scaled\&BBCNRW\_live\&|zbbc|<10cm}}{N^i_{BBCNRW\_scaled\&ERTC\_live\&|zbbc|<10cm}} \times \frac{N^i_{BBCNRW\_scaled\&|zbbc|<10cm}}{22.9mb} = 2.8886pb^{-1} \quad (2.1)$$

2.3 $\pi^{\pm}$ Identification Cuts

- $|BBCZ| < 30$cm
- ERT4x4C trigger
- 5 $GeV/c < pT < 15$ GeV/c for ERT4x4C
- DCQuality == 31 || DCQuality == 63
- -70cm $< DCZed <$ 70cm
- $0.2 < emce/p < 0.8$
- Shower Shape to be EM (prob) < 0.1
- RICH n1 > 0
- $|CalibratedEMCal| < 3$

- $|CalibratedEMCalz| < 3$

Chapter 3

QA and Calibration

Run and Fill QA and Calibration by using all detectors and Spin information.

3.1 Warn Map in the EMCal

EMCal detectors have continuous hot and dead channels. It need to mask for getting pure event.

3.2 Dead Maps for DC, PC and RICH

In Charged Pion analysis, DC, PC, RICH Detector also used. They have continuous dead channels. It need to mask for getting pure event, respectively.

3.3 Fiducial Cuts in the Central Arm

TSSA measurements in p + p collisions are best described with twist-3 collinear correlation functions which can describe spin-momentum correlations both in the proton and in the process of hadronization. $\pi^+ = u\bar{d}$, $\pi^- = d\bar{u}$) the $\pi^{\pm}$. Because they are hadrons, they are sensitive to both initial- and final-state effects. Unlike at forward rapidity, midra-

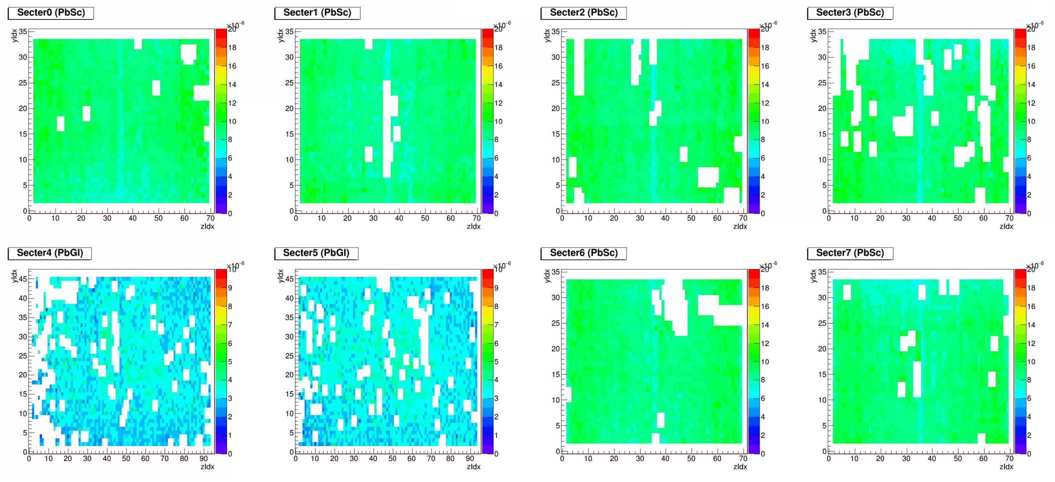

Figure 3.1: EMCal 8 sectors warnmap.

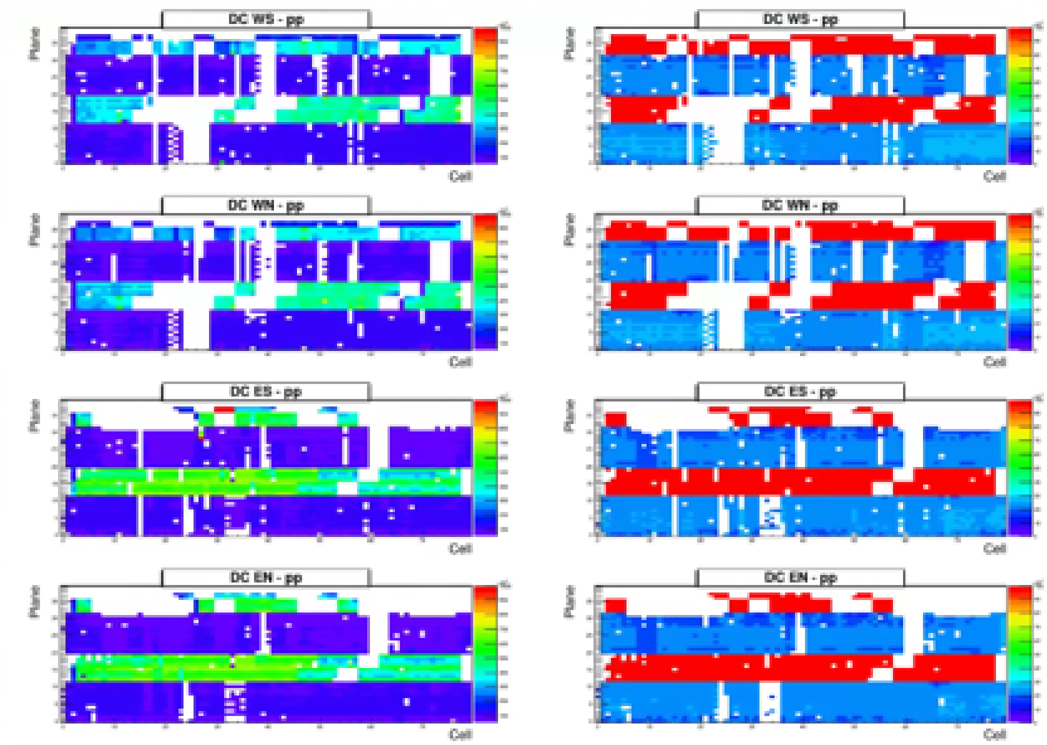

Figure 3.2: Drift Chamber Deadmap.

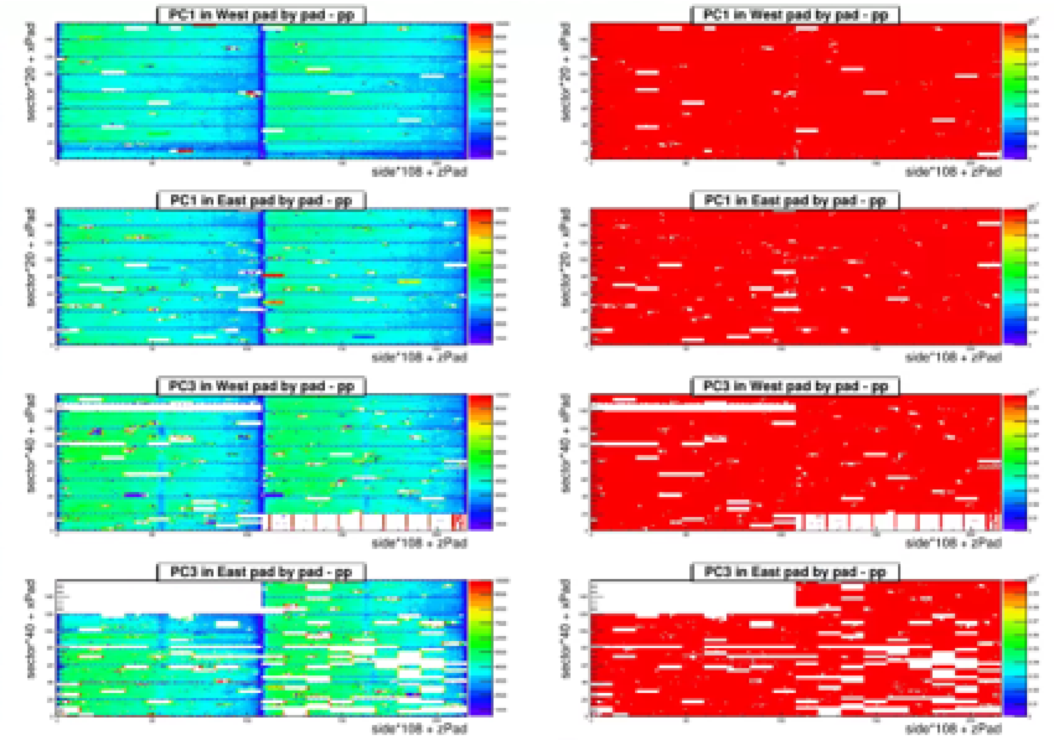

Figure 3.3: Pad Chamber Deadmap.

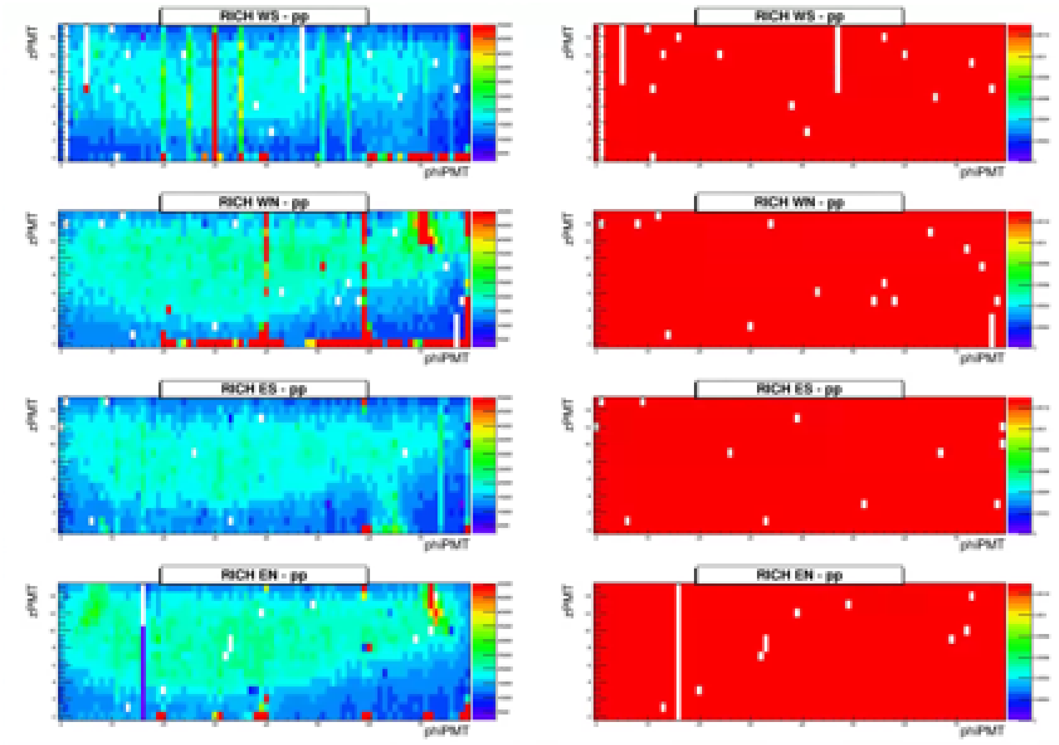

Figure 3.4: RICH Deadmap.

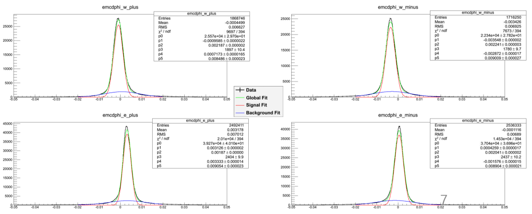

(a) emcdphi and emcdz distribution before Matching Calibration

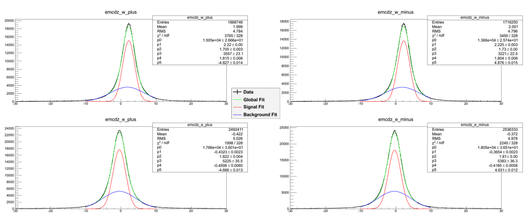

(b) emcdphi and emcdz distribution before Matching Calibration

Figure 3.5: ROC curve of failure detection

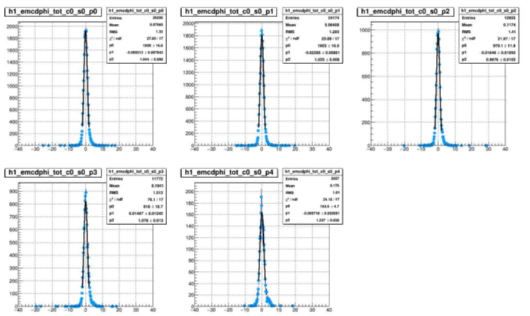

(a) emcdphi and emcdz distribution after Matching Calibration

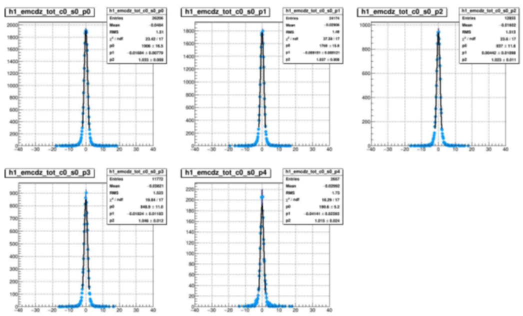

(b) emcdphi and emcdz distribution after Matching Calibration

Figure 3.6: ROC curve of failure detection

pidity π 0s are sensitive at leading order to gluon spin-momentum correlations both in the proton and in the process of hadronization.

3.4 Matching Calibration in the EMCal and PC3

3.5 Polarization

For this analysis, polarization information will use to calculate A_N

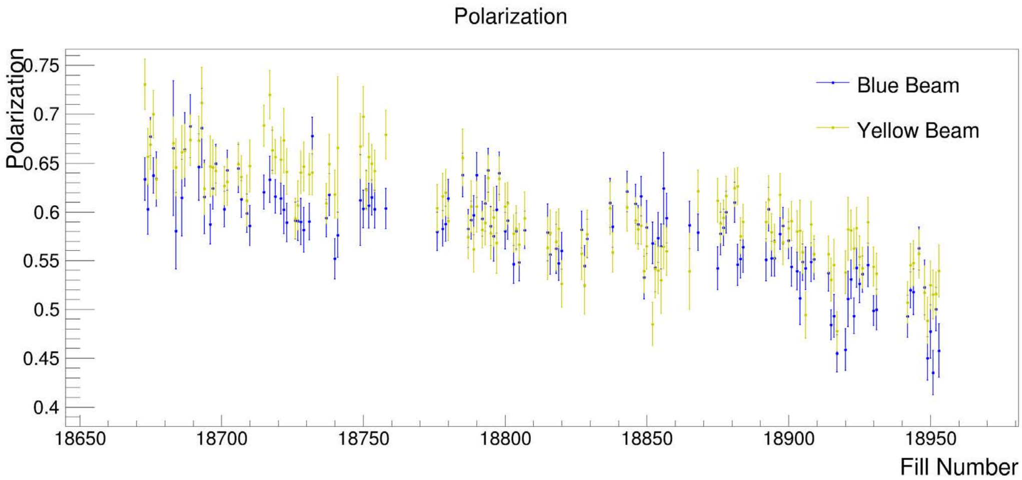

Figure 3.7: Run 15 pp collision Polarization by fill.

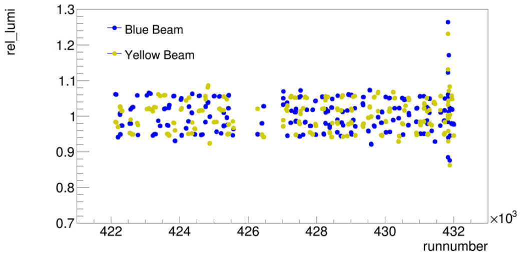

(a) Relative Luminosity run by run

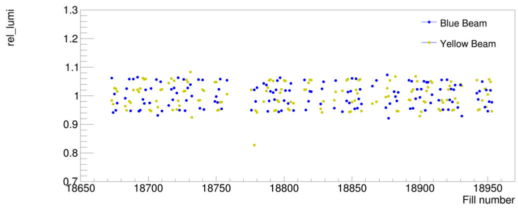

(b) Relative Luminosity fill by fill

Figure 3.8: Run 15 pp collision Relative Luminosity fill by fill and run by run.

3.6 Relative Luminosity

For this analysis, Relative Luminosity will use to calculate A_N by Relative Luminosity Formula

3.7 Azimuthal Correction

Raw A_N follows the shape of the cos function. Azimutal Acceptance Correction Factor is the amplitude of cos function.

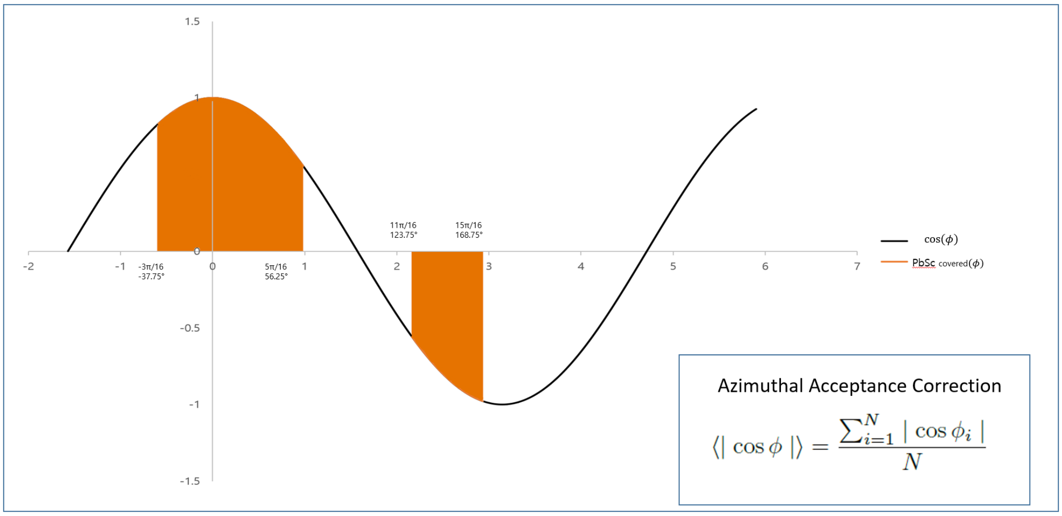

Figure 3.9: Approximate appearance of Raw A_N and Azimuthal Acceptance Correction Formula.

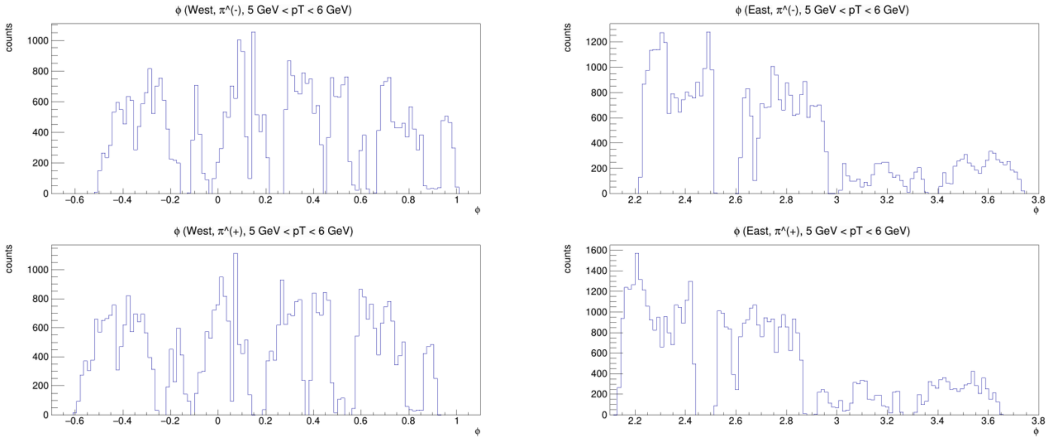

Figure 3.10: phi distribution in 5 ∼ 6 GeV pT range

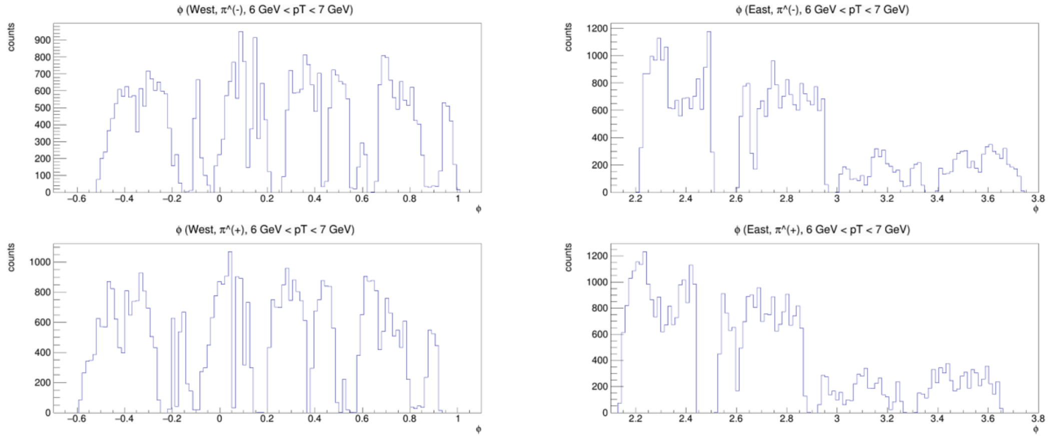

Figure 3.11: phi distribution in 6 $\sim$ 7 GeV pT range

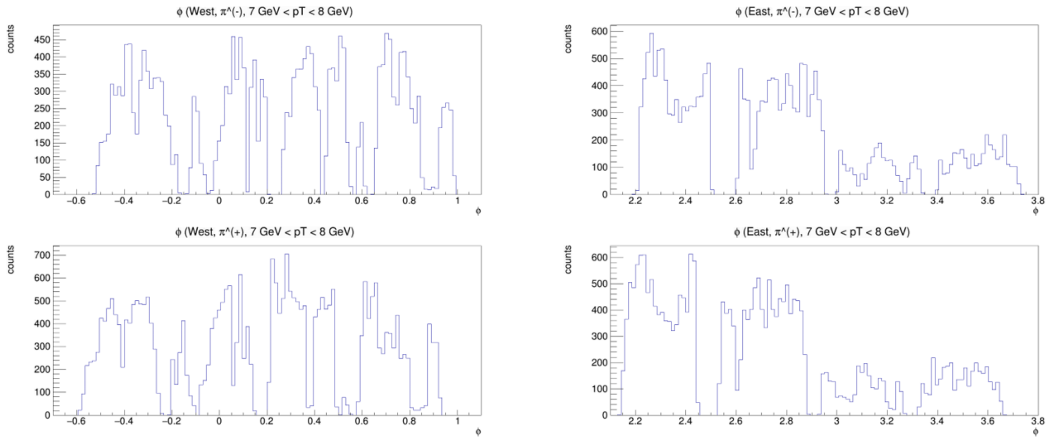

Figure 3.12: phi distribution in 7 $\sim$ 8 GeV pT range

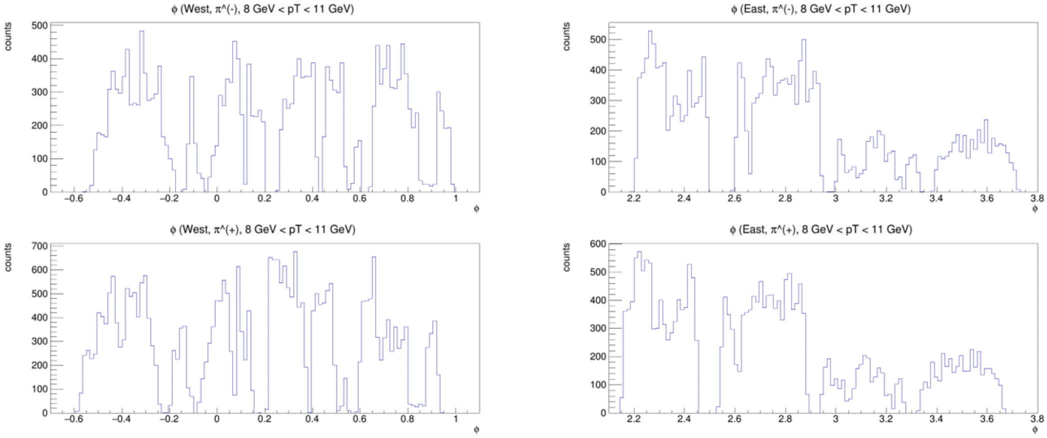

Figure 3.13: phi distribution in 8 $\sim$ 11 GeV pT range

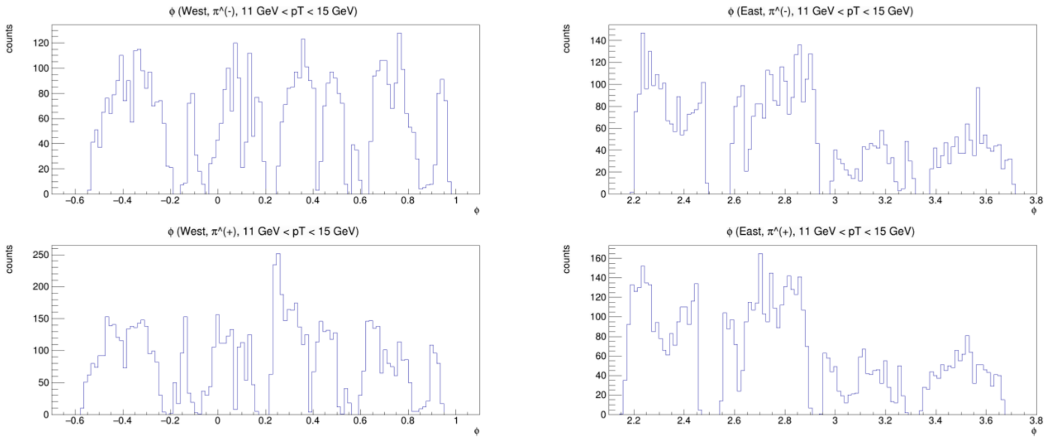

Figure 3.14: phi distribution in 11 $\sim$ 15 GeV pT range

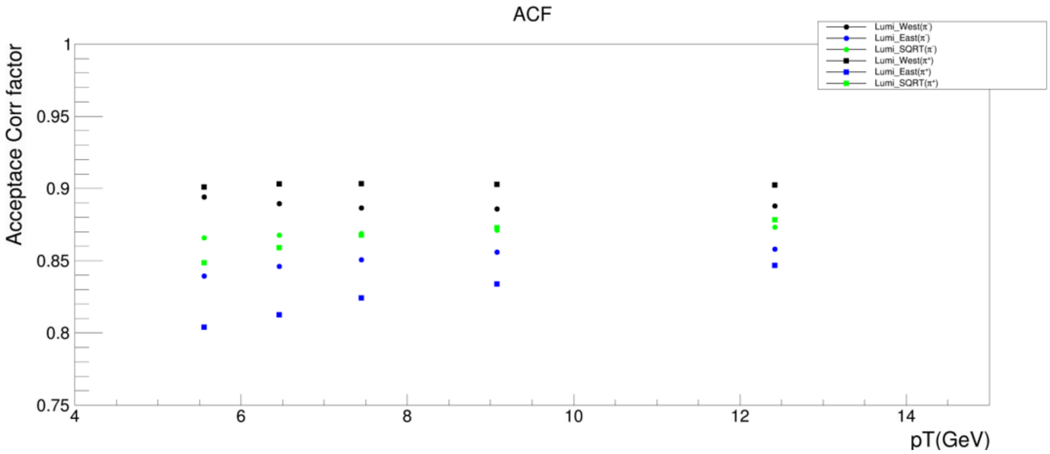

Figure 3.15: Azimutal Acceptance Correction Factor for Both Arms used for the square root formula and Relative Luminosity Formula in East and west arm, respectively.

Chapter 4

Cross Section Analysis

Cross section is useful to check that this result from data is enough good or not.

4.1 $\pi^{\pm}$ Yields Extraction

In pion analysis, Electrons, Kaons and prontons still remain after apply pion PID cut. The red line is estimated to be the background and I will calculate background by using Pythia simulation, minutely.

4.2 Acceptance X Reconstruction Efficiency

PHENIX Detector System have own acceptance and each detector have own efficiency. For calculating

4.3 Trigger Efficiency

To calculate ERT 4x4c trigger efficiency, All dataset is needed for statistics.

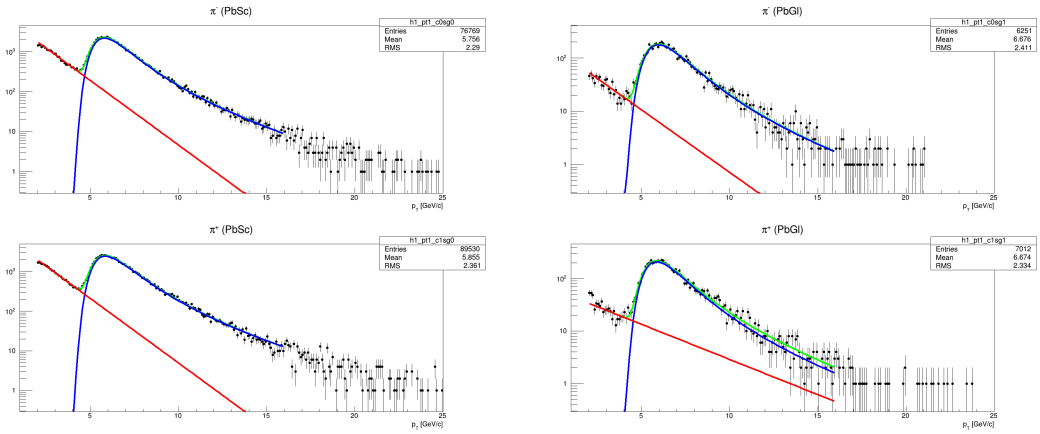

Figure 4.1: $\pi^{\pm}$ Yields Extraction for run15 pp collision in central arm.

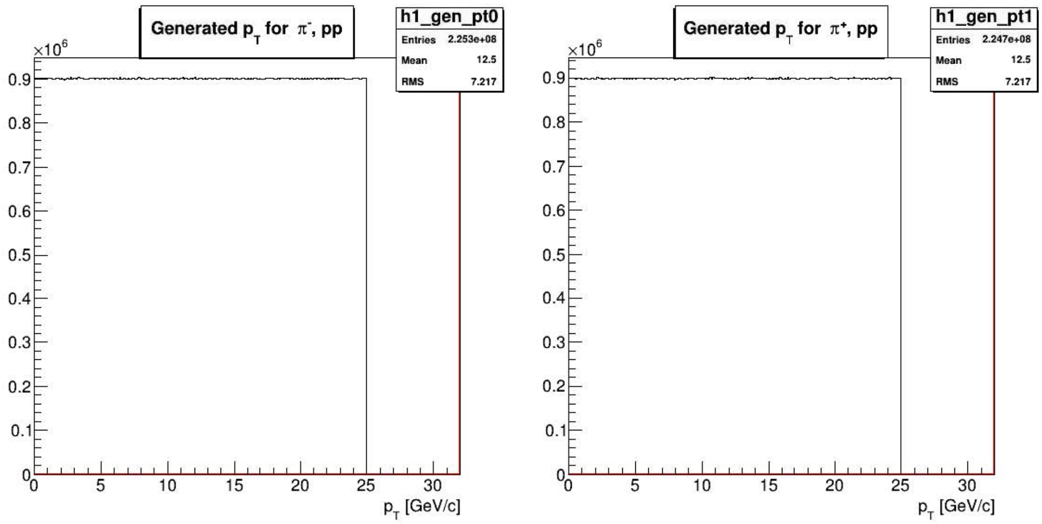

Figure 4.2: Generated $\pi^{\pm}$ distribution by using single particle generator.

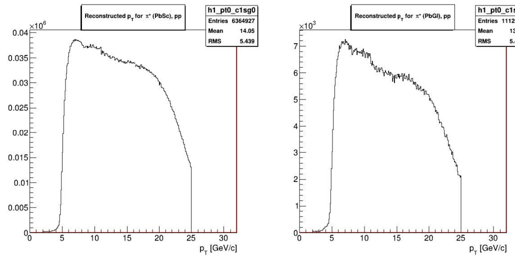

(a) Reconstructed π^+. as function of pT.

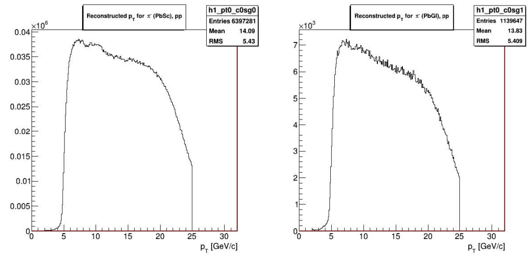

(b) Reconstructed π^-. as function of pT.

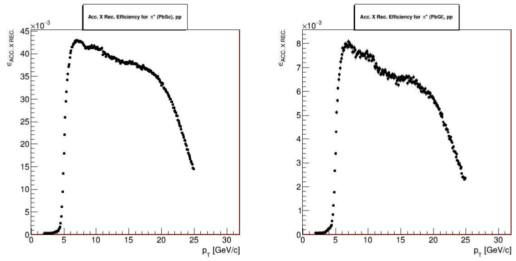

(c) Rec. X Acc. efficiency for π^+.

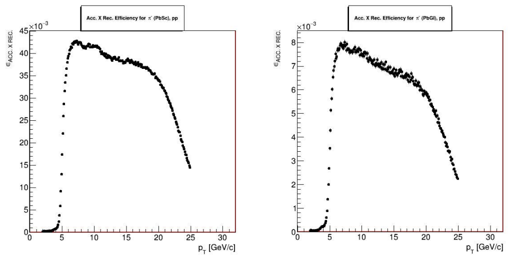

(d) Rec. X Acc. efficiency for π^-.

Figure 4.3: Rec. X Acc. efficiency for $\pi^{\pm}$ by simulation.

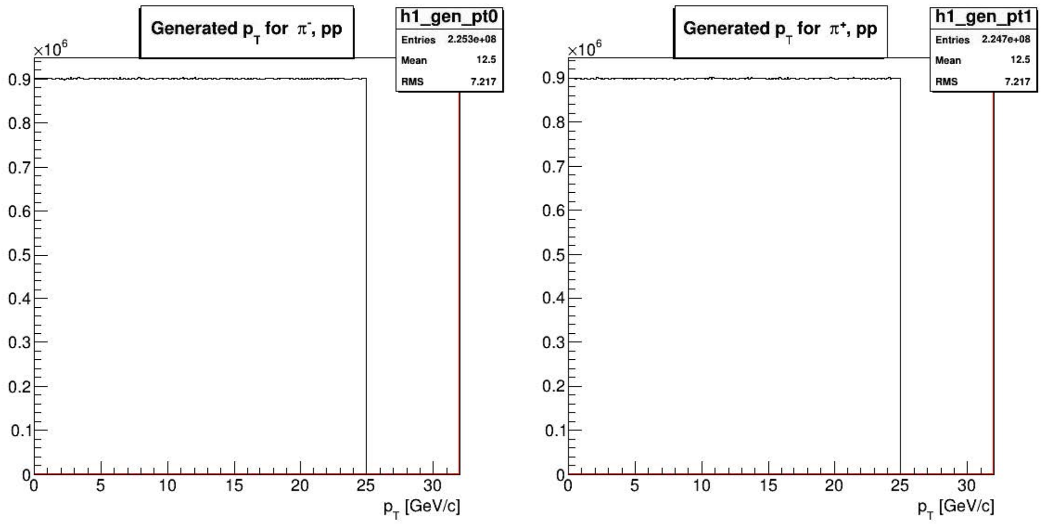

Figure 4.4: Generated $\pi^{\pm}$ distribution by using single particle generator.

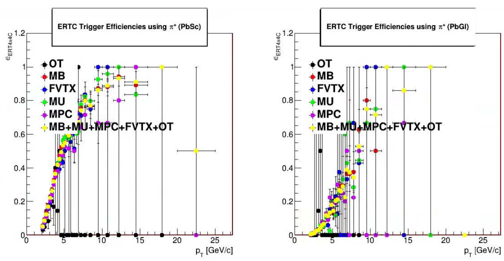

(a) trigger efficiency for π^+.

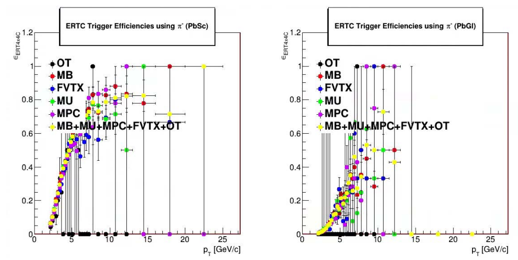

(b) trigger efficiency for π^-.

Figure 4.5: trigger efficiency for $\pi^{\pm}$ compared each dataset

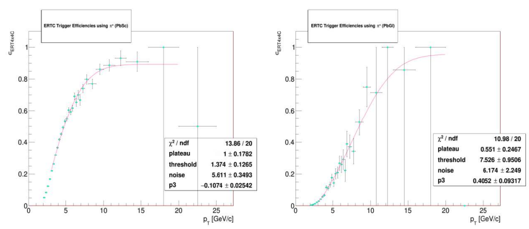

(a) trigger efficiency for π^+.

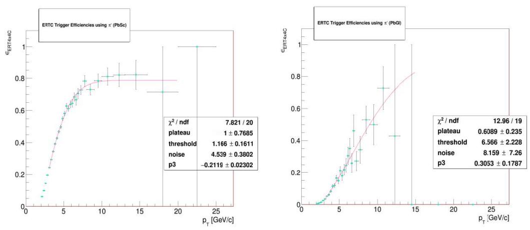

(b) trigger efficiency for π^-.

Figure 4.6: trigger efficiency for $\pi^{\pm}$ with all dataset.

4.4 Results

This is Cross Section for Charged Pion in Run15 200Gev pp collision.

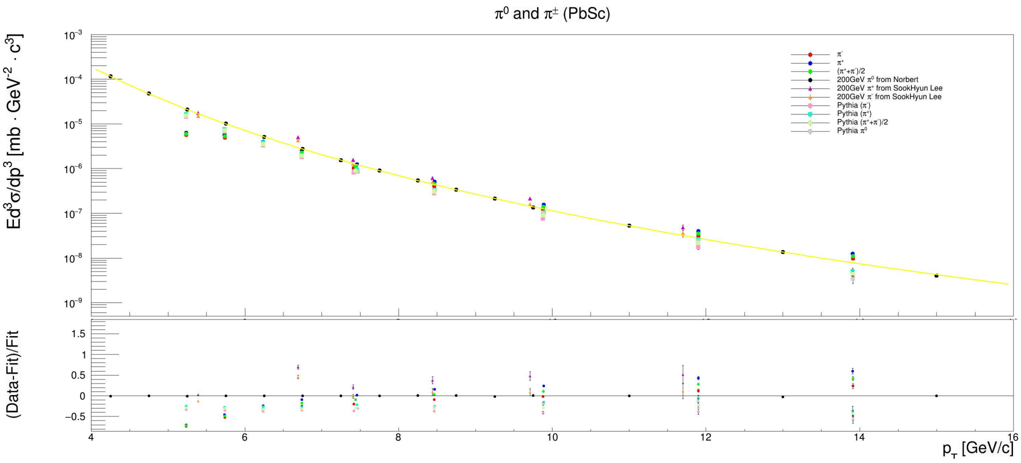

Figure 4.7: Cross Section for $\pi^{\pm}$ with Yuehang's 200GeV configuration file by using Pythia simulation.

Chapter 5

A_N Analysis

5.1 A_N Calculation

We use two kinds of A_N Calculation formula.

5.1.1 Mean p_T

Mean p_T used for center of each p_T region.

Particle	p_T *bin* (GeV/c)	$Mean\ p_T(GeV/c)$
	$5 \sim 6$	5.55619
	$6 \sim 7$	6.46008
$\pi^{\pm}$	$7 \sim 8$	7.44575
	$8 \sim 11$	9.07912
	$11 \sim 15$	12.4215

Table 5.1: Finalized cut values, FoM

$$A_N^{raw} = \frac{\sqrt{N_L^{\uparrow} N_R^{\downarrow}} - \sqrt{N_L^{\downarrow} N_R^{\uparrow}}}{\sqrt{N_L^{\uparrow} N_R^{\downarrow}} + \sqrt{N_L^{\downarrow} N_R^{\uparrow}}}$$

$$\sigma_{A_N^{raw}} = \frac{\sqrt{N_L^{\uparrow} N_R^{\downarrow} N_L^{\downarrow} N_R^{\uparrow}}}{(\sqrt{N_L^{\uparrow} N_R^{\downarrow}} + \sqrt{N_L^{\downarrow} N_R^{\uparrow}})^2} \sqrt{\frac{1}{N_L^{\uparrow}} + \frac{1}{N_L^{\downarrow}} + \frac{1}{N_R^{\uparrow}} + \frac{1}{N_R^{\downarrow}}}$$

Figure 5.1: Square Root Formula.

5.1.2 Square Root Formula

Square Root Formula can use without Relative Luminosity and it have more statistics while averaging fills.

5.1.3 Relative Luminosity Formula

Relative Luminosity Formula can use only respective sections or regions.

5.1.4 $sin\phi$ Modulation Cross Check

this cross check is not using Azimutal Acceptance Correction when A_{N_raw} calculated. I use fitting function to calculate A_{N_raw}.

$$A_N^{raw} = \frac{N_L^{\uparrow} - \mathcal{R}\, N_L^{\downarrow}}{N_L^{\uparrow} + \mathcal{R}\, N_L^{\downarrow}}$$

$$\sigma_{A_N^{raw}} = \frac{2\,\mathcal{R}\, N_L^{\uparrow} N_L^{\downarrow}}{(N_L^{\uparrow} + \mathcal{R}\, N_L^{\downarrow})^2} \sqrt{\frac{1}{N_L^{\uparrow}} + \frac{1}{N_L^{\downarrow}}}$$

Figure 5.2: Relative Luminosity Formula.

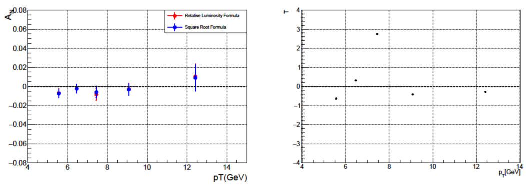

(a) A_N for π^+.

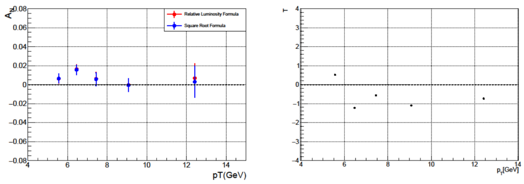

(b) A_N for π^-.

Figure 5.3: A_N from different formula.

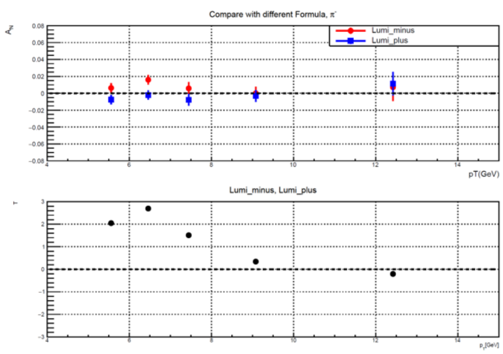

(a) A_N for π^+.

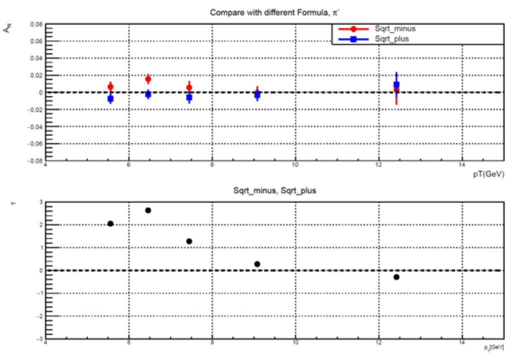

(b) A_N for π^-.

Figure 5.4: A_N compare with different charge.

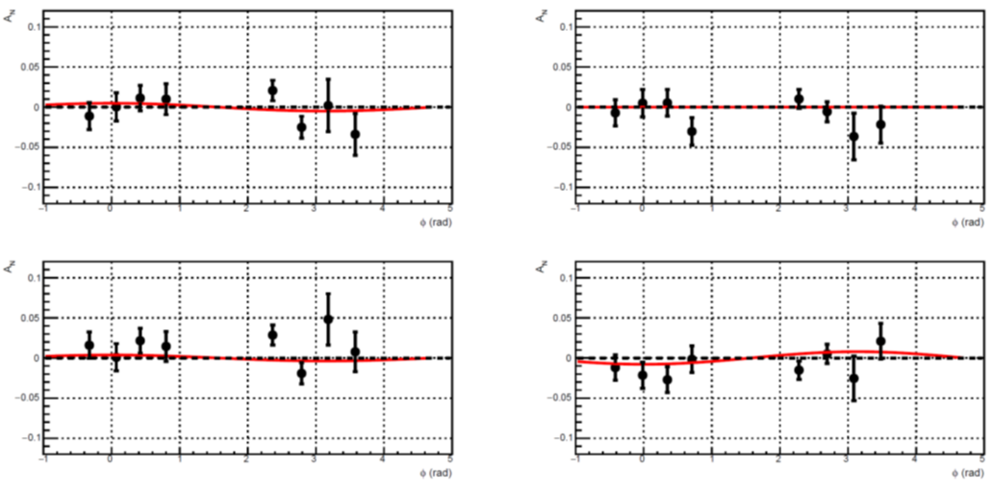

Figure 5.5: Asymmetry as a function of ϕ for $5 < pT < 6$ GeV.

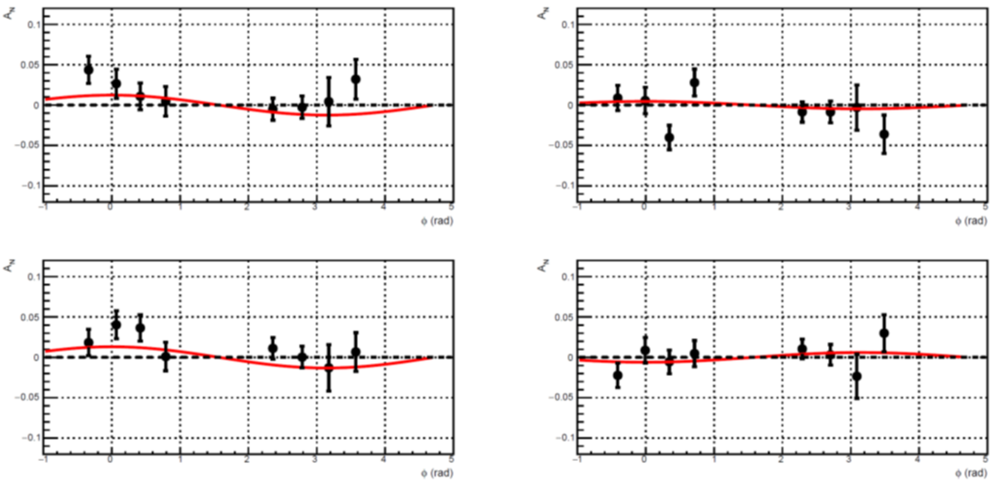

Figure 5.6: Asymmetry as a function of ϕ for $6 < pT < 7$ GeV.

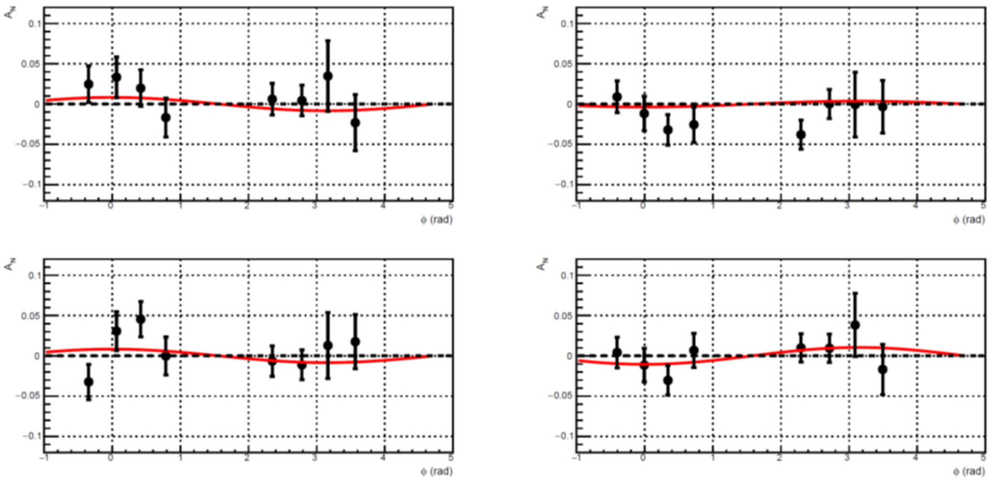

Figure 5.7: Asymmetry as a function of ϕ for $7 < pT < 8$ GeV.

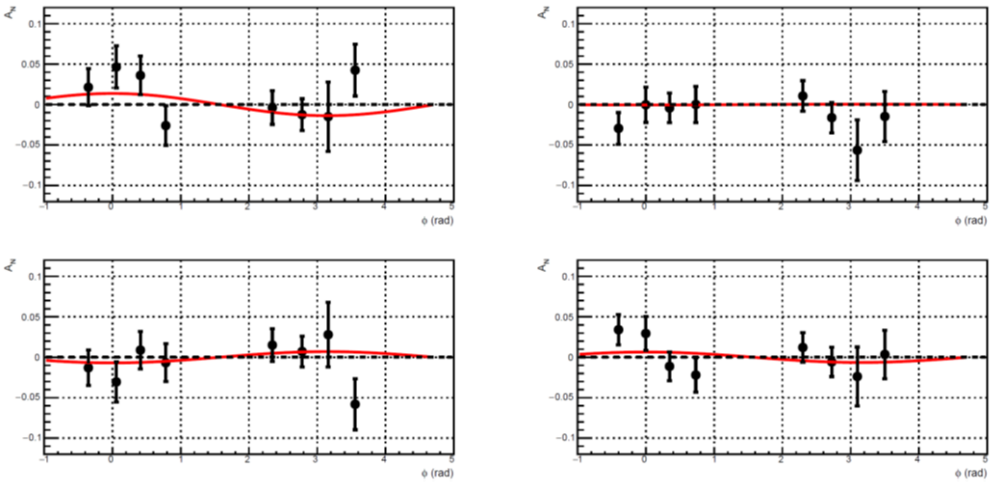

Figure 5.8: Asymmetry as a function of ϕ for $8 < pT < 11$ GeV.

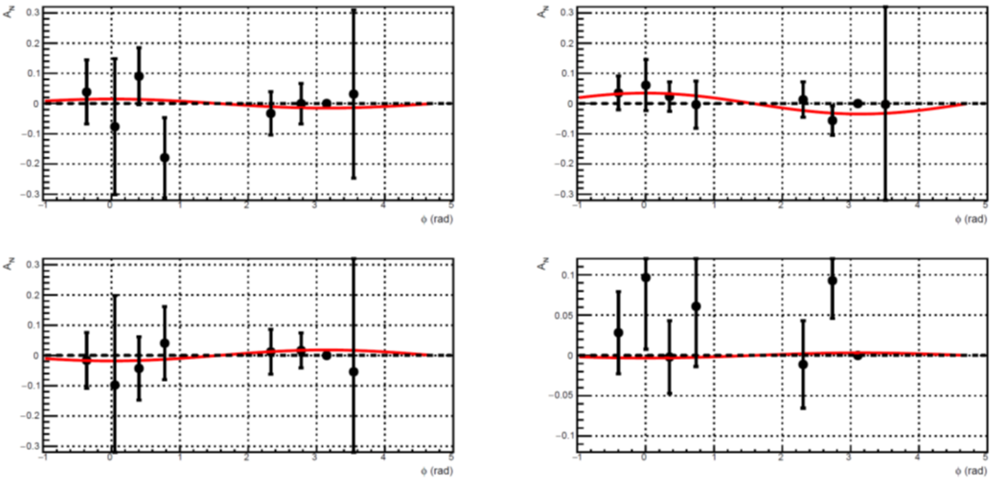

Figure 5.9: Asymmetry as a function of ϕ for $11 < pT < 15\ GeV$.

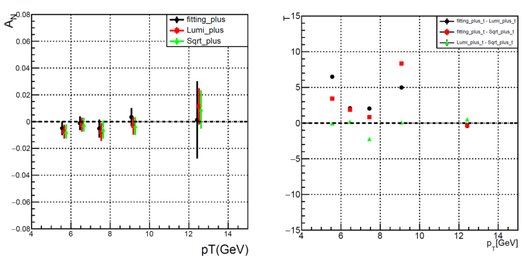

(a) A_N Cross Check for π^+.

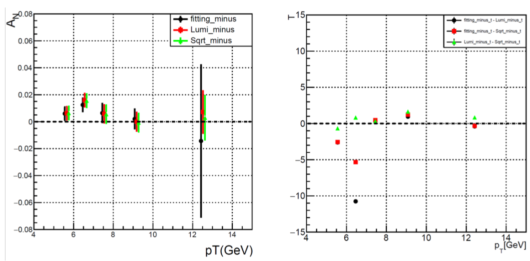

(b) A_N Cross Check for π^-.

Figure 5.10: A_N Cross Check.

5.2 Background Subtraction

5.2.1 Background Fraction

Hadron Background

Electron Background

5.2.2 Background Asymmetry

5.2.3 Results After Background Correction

Chapter 6

Systematic Studies

6.1 Uncertainty of Relative Luminosity

6.2 Global Scaling Uncertainty from Polarization

6.3 Bunch Shuffling

6.4 False Asymmetry from Ghost Cluster in the EMCal

6.5 Uncertainty from Background

6.6 Final Result

Chapter 7

Conclusion

This is the conclusion.

7.1 The Section

Bibliography